

Soft Kirigami Composites for Form-Finding of Fully Flexible Deployables

Jan Zavodnik, Yunbo Wang, Wenzhong Yan, Miha Brojan,*
and Mohammad Khalid Jawed*

A new class of thin flexible structures is introduced that morph from flat into prescribed 3D shapes through strain mismatch between layers of a composite plate. To achieve control over the target shape, two different concepts are coupled. First, motivated by biological growth, strain mismatch is applied between the flat composite layers to transform it into a 3D shape. Depending on the amount of the applied strain mismatch, the transformation involves buckling into one of the available finite number of deformation modes. Second, inspired by kirigami, portions of the material are removed from one of the layers according to a specific pattern. This dramatically increases the number of possible 3D shapes and allows us to attain specific topologies. An experimental apparatus that allows precise control of the strain mismatch is devised. An inverse problem is posed, where starting from a given target shape, the physical parameters that make these shapes possible are determined. To show how the concept works, it focuses on circular composite plates and designs a kirigami pattern that yields a hemispherical structure. The analysis combines a theoretical approach with numerical simulations and physical experiments to understand and predict the shape transition from 2D to 3D. The tools developed here can be extended to attain arbitrary 3D shapes. The initially flat shape suggests that conventional additive manufacturing techniques can be used to functionalize the soft kirigami composite to fabricate, for example, deployable 3D structures, smart skins, and soft electromagnetic metasurfaces.

scales from microns^[1] to meters.^[2] Since conventional additive and subtractive manufacturing techniques typically support planar fabrication, morphing from 2D to 3D is a promising way to achieve 3D functional surfaces for use in, e.g., curvy electronics for wearables,^[3] camouflaging,^[4] structural health monitoring,^[5] multi-functional soft machines,^[6] with existing manufacturing tools. Since the introduction of bimetallic strips^[7] in the 18th century, morphing of slender structures into desired shapes has been actuated via heat,^[8,9] swelling,^[10,11] light,^[12] electromagnetism,^[13] chemical gradient,^[14] pneumatics,^[15] growth,^[16] material anisotropy,^[17] tailored material removal,^[18–20] and other forms of external stimuli. Another approach to morphing is inspired by origami, which has been particularly successful in deployable aerospace structures^[21] that require small storage space but a large surface area. Such deployables are typically piecewise rigid and may require multiple springs, support structures, or other mechanisms for deployment. In this paper, a new class of deployables


are envisioned that morph, upon release of constraints, from a planar shape to a prescribed 3D structure and are fully flexible without any rigid parts. Note that our soft kirigami composite once transformed to 3D upon release of the constraints applied

1. Introduction

Morphing planar shapes into preprogrammed 3D structures has applications in engineering across a wide range of length-

J. Zavodnik, M. Brojan
Faculty of Mechanical Engineering
Laboratory for Nonlinear Mechanics
University of Ljubljana
Aškerčeva 6, Ljubljana SI-1000, Slovenia
E-mail: miha.brojan@fs.uni-lj.si

Y. Wang, W. Yan, M. K. Jawed
Los Angeles
Department of Mechanical and Aerospace Engineering
University of California
420 Westwood Plaza, Los Angeles, CA 90024, USA
E-mail: khalidjm@seas.ucla.edu

 The ORCID identification number(s) for the author(s) of this article can be found under <https://doi.org/10.1002/admt.202300909>

© 2023 The Authors. Advanced Materials Technologies published by Wiley-VCH GmbH. This is an open access article under the terms of the Creative Commons Attribution-NonCommercial License, which permits use, distribution and reproduction in any medium, provided the original work is properly cited and is not used for commercial purposes.

DOI: 10.1002/admt.202300909

during the fabrication can be stretched back to regain a perfectly flat shape without any Poisson effects. This can be very effective for transportation and applications in space engineering, since the structure already carries the energy for self-deployment.

Toward fully flexible shells that morph from a 2D shape to a prescribed 3D topology, previous works on imposing mechanical loads and boundary conditions on sheets provide a solid foundation. Simply pulling a thin elastic sheet can induce 3D deformation through wrinkling instabilities.^[22] Grason et al. showed that imposing curvature to elastic sheets leads to distinct types of structural instabilities.^[23] We consider this as an *incompatibility* of topologies leading to complex structures. A simple instantiation of this concept can be achieved by draping a flat cloth around a spherical object. If the radius of the sphere is much larger than the size of the cloth, the planar cloth may assume the imposed 3D topography. However, if the sizes of the cloth and the sphere are comparable, wrinkles, and crumples form. Geometric frustration leading to mechanical instabilities in sheets manifests itself in geometrically incompatible confinement of solids. Davdovitch et al.^[24] studied a class of such problems in which the topography imposed on a thin solid body is incompatible with its intrinsic metric and wrinkles emerged as a consequence. To construct a specific 3D shape from sheets and avoid wrinkling, carefully targeted portions of the material can be removed to relieve these geometric frustrations, as shown e.g., in ref. [25, 26]. These earlier works on the type and size of patterns during 2D to 3D transition inspired our solution to obtain 3D structures with a prescribed target metric. Specifically, to avoid wrinkles (which depend on geometry and material stiffness) on the 3D structure, we explore the removal of the material to relieve geometric frustration and study its dependence on geometric and material properties.

New possibilities for shape selection open up when strain mismatch is introduced within a flat structure.^[27–31] Pezzulla et al.^[30] studied geometric frustration between multiple parts of the body that leads to 3D deformation of the naturally planar object. Strain mismatch introduced into any part of a thin body by, e.g., heating, growth, or swelling, can drastically affect the morphology of the entire object and induce mechanical instabilities. Such morphological changes are preponderant in biological structures and are often necessary for their functionality; examples include Venus flytrap, growing leaves, and the writhing of tendrils bearing climbers in plants and formation of brains, lungs, and guts in animals. Combining geometric confinement with strain mismatch can open pathways to an even broader class of topographies. Stein et al.^[32] used residual swelling and geometric confinement to generate a range of structures including saddles, rolled sheets, cylinders, and spherical sections. Our work synergistically combines emergence of mechanical instabilities and strain mismatch to fabricate composite shells that morph from a flat shape to a prescribed 3D form.

In this paper, we emphasize having control over the final 3D shape that forms by morphing from an initially planar shape. Examples of different 3D topographies that can be obtained using our procedure are provided in the Figure S1 (Supporting Information). Our work uses a hemisphere as a representative 3D shape to observe transformation of a flat space into one with non-negative Gaussian curvature. An intuitive (but ultimately incor-

rect) approach is presented in **Figure 1A**, where a “bottom” layer is radially stretched and attached to a “top” unstretched layer to form a soft composite shell. The shape of this composite is 3D but not hemispherical. A number of distinct shapes can emerge in this system, which are analyzed via physical experiments on soft materials, numerical simulations using the finite element method and theoretical deliberations based on plate and shell theories. This lays the foundation for a solution to the hemispherical problem. Kirigami (i.e., removal of material) to relieve geometric frustration is introduced; a combination of kirigami and strain mismatch is proposed to access arbitrary 3D shapes. **Figure 1B** shows an example where a hemispherical shape is achieved by tuning the kirigami pattern and the strain mismatch. A new experimental apparatus is designed and fabricated to impose uniform biaxial stretch onto the bottom layer while avoiding wrinkling due to Poisson’s effect.^[33]

Our paper is organized as follows. We commence with a description of the experimental apparatus in *Physical Experiments*. Various shapes resulting from two circular layers with strain mismatch is described in *Soft Circular Composites*. Application of kirigami on this composite is introduced in *Soft Kirigami Composites* and methods to achieve the target hemispherical shape are discussed there.

2. Experimental Section

A snapshot of the custom designed experimental apparatus is presented in **Figure 2(A1–A2)**. Two main components – a 3D-printed cylinder assembly and two vertically positioned linear translation stages – make up the set. The hyperelastic materials of the bottom layer (VHB 4910, 3M) and the top layer (VHB 4950, 3M) had double-side stickiness. Material properties are listed in Section 2.1. As shown in **Figure 2(A2)**, the bottom layer was placed on top of the cylindrical casing. The contacting part was pressed by a 3D-printed gripper in **Figure 2(B1–B2)**. The assembly was then placed between two vertical linear translation stages and the stages were moved to a specific height corresponding to a specific prestretch. As the stages were moved upward, the piston – pushed by the height adjuster – also moved up but the outer edge of the bottom layer remains gripped onto the cylindrical casing. This leads to a uniform biaxial stretch in the hyperelastic material. The relation between the imposed stretch and height could be determined from simple geometry. The top layer was glued onto the stretched bottom layer to form a bilayer composite. The bilayer composite was then cut out from the apparatus and released from the gripper. This resulting 3D structure was referred to as the “soft kirigami composite” in this paper.

2.1. Physical Parameters

A commercially available acrylic adhesive (3M VHB tape) was used as the bottom and kirigami layers. Mooney-Rivlin model was used in the finite element simulations of **Figure 3** and **Figure 5**. The strain energy per unit of reference volume in this model is

$$U = C_1(\bar{I}_1 - 3) + C_2(\bar{I}_2 - 3) + D_1(J - 1)^2 \quad (1)$$

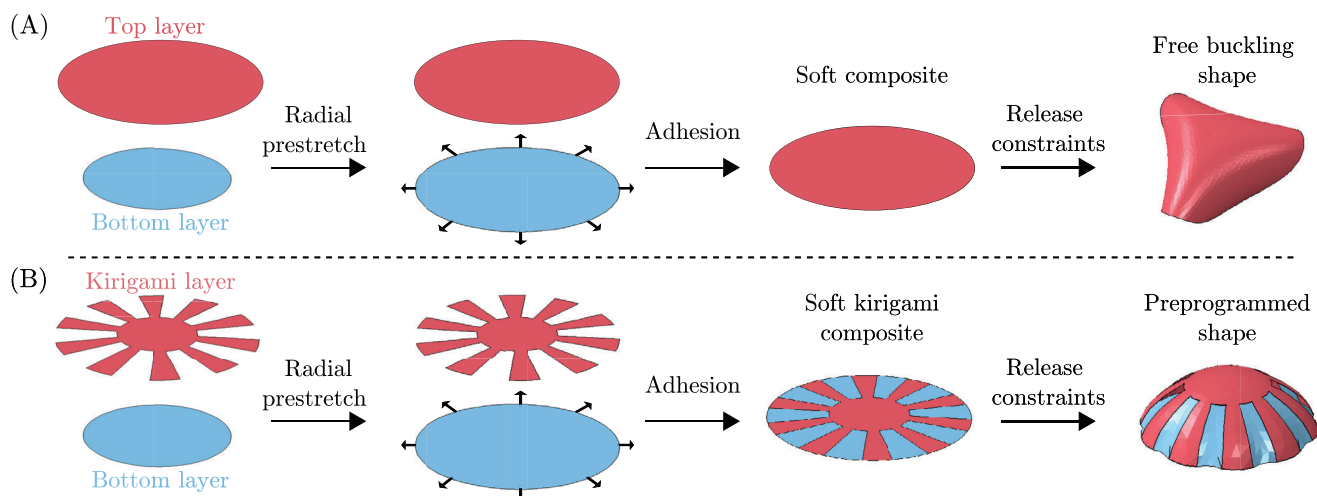


Figure 1. Overview of the problem. A) Of two circular layers, the bottom layer is stretched and adhered to the unstretched top layer to obtain a soft composite. Upon releasing the constraints, the strain mismatch between the two layers induces symmetry breaking and the composite may assume a buckled shape with a finite number (*three* in this case) of waves along the circumference. B) Replacing the top circular layer with a kirigami layer (layer with cuts) can lead to a preprogrammed shape via the same procedure. The shape is governed by the kirigami pattern. In this case, the goal was to obtain an axisymmetrical cap.

where C_1 , C_2 , and D_1 are material parameters, \bar{I}_1 and \bar{I}_2 are the first and second deviatoric strain invariants, and J is the elastic volume ratio.^[34] The bottom layer has a thickness of $h = 1.0$ mm and its material parameters are $C_1 = 4.84$ kPa, $C_2 = 14.536$ kPa, and $D_1 = 0.96 \times 10^3$ kPa. The kirigami/top layer is $h = 1.1$ mm thick with the following material parameters: $C_1 = 4.00$ kPa, $C_2 = 78.7152$ kPa, and $D_1 = 4.1082 \times 10^3$ kPa.

In order to normalize the elastic strain energy, it formulated a characteristic elastic energy of the composites: $E^* = Yh^3$, where $Y = 2G(1 + \nu)$ is the effective Young's modulus of the substrate, h is the thickness of the substrate, and $\nu = (3K - 2G)/(6K + 2G)$, $G = 2(C_1 + C_2)$, and $K = 2D_1$. The behavior of both materials in an uniaxial and biaxial test is presented in Section S2 (Supporting Information) to show that a linear approximation is reasonable. For the soft kirigami composites in Figure 5, the number of cuts is $n_c = 10$, the ratio of the inner radius (r_i in Figure 5A) to the outer radius (r_o) is $\bar{r} = 0.4$, and the cutout angle is $d\theta = 0.1$ radians, i.e., 1 out of 2π radian was removed. This corresponds to portion of the removed material $\alpha = 0.13$.

3. Soft Circular Composites

Our investigation starts with the setup described in Figure 1. A bottom layer of circular shape is first stretched by a prescribed amount of prestretch $\lambda > 1$ ($\lambda = 1$ corresponds to stress-free configuration). A stress-free circular top layer is affixed onto the bottom layer. Physical parameters are described in Section 2.1. Once the composite structure is released from the experimental setup of Figure 2, a variety of shapes emerge depending on the prestretch, λ . In Figure 3A, a series of four shapes of the experimental composites are presented. These shapes – that only differ by λ – are qualitatively different. The number of wrinkles on the outer edge of the composites, represented by the k number in the figure, increases from $k = 0$ in Figure 3A1 to $k = 4$ in Figure 3A4. Figure 3B shows finite element simulations that can also cap-

ture the qualitatively distinct shapes. While developing FE simulations, we realized the existence of different branches in the solution space and a propensity for the FE method to reach a local energy minimum instead of the global. Section S6 (Supporting Information) provides details on the techniques used to address this issue. This exposes a challenge in numerical simulation of such structures and motivates us to fundamentally understand the problem through a theoretical lens. The next section outlines the theory that was developed to explain the observations in Figure 3.

4. Composite Plate Theory

With the following theory we reduce the complexity of the problem and analyze the main phenomena that occur in the prestretched composite plate during morphing. We assume plane stress and Kirchhoff kinematic assumption on total in-plane displacement as the circular laminated composite plates used in experiments are thin.^[35] We use the Green-Lagrange (GL) strain tensor under Föppl-von Karman (FvK) kinematic assumptions, which further simplifies the theory and limits it to small strains and moderate rotations. Without loss of physical insight we approximate the (otherwise hyperelastic, cf. Equation (1)) material response with the St. Venant-Kirchhoff elastic material model

$$\sigma_K = \frac{Y_K}{1 - \nu_K^2} \left((1 - \nu_K)(E_{FvK} - S_K) + \nu_K \text{tr}(E_{FvK} - S_K)I \right) \quad (2)$$

where σ_K , E_{FvK} , Y_K , ν_K , S_K are the Cauchy stress, strain under the FvK assumptions, Young modulus, Poisson ratio, and pre-strain tensor in K -th layer in the composite, respectively. As in experiment, we apply the strains due to prestretch $S_K = -I(\lambda - 1)$, where λ and I are the applied prestretch and a unity matrix, respectively. We define a membrane force and bending moment

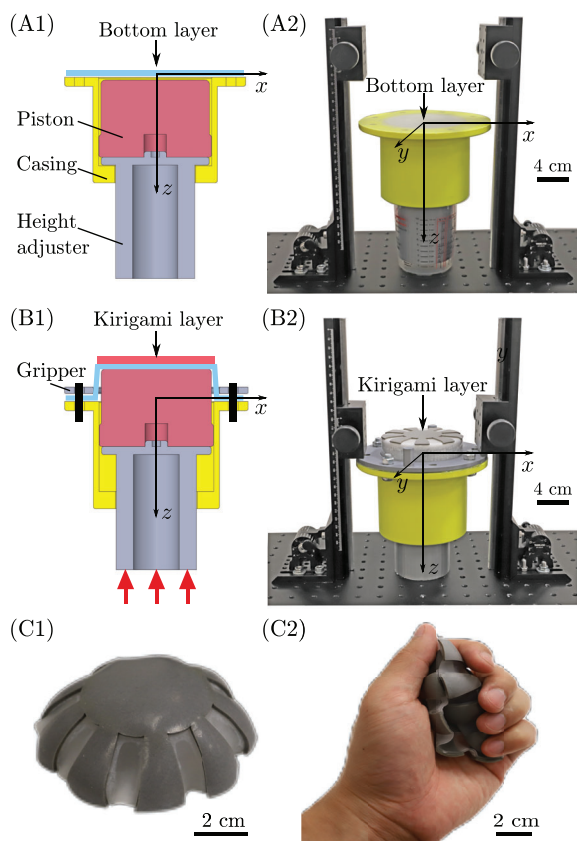


Figure 2. Experimental system. A1) Schematic representation of the experimental system comprised of piston, casing, height adjuster, and annulus-shaped gripper. The bottom layer is attached above the piston. A2) Snapshot of the system when bottom layer is still unstretched. B1) Bottom layer is stretched by raising the piston along the z -axis and the kirigami layer is adhered on top. B2) Snapshot of the system with soft kirigami composites still under constraints. C1) After the constraints are removed by cutting the bottom layer from the gripper, the soft kirigami composite assumes the shape of a (quasi)axisymmetrical cap. C2) The resulting composite is fully (elastically) flexible. It can be orderly folded or crumpled and thus stored in confined spaces, yet it returns to its preprogrammed shape upon the release of constraints.

tensors (both per unit length) by integrating the section stresses and section stresses weighted by a distance from the reference plane through the thickness of the composite, respectively. This is a classical procedure, yet due to multiple number of different layers and prestretched layers it yields different results than those in the classic shell theory. In our case both the membrane forces \mathbf{N} and the bending moments \mathbf{M} are functions of the curvature tensor $\boldsymbol{\kappa}$, in-plane strain tensor $\mathbf{E}_{\text{FvK}}^0$ and most importantly the prestretch λ

$$\begin{aligned} \mathbf{N} &= \bar{\boldsymbol{\alpha}} \mathbf{E}_{\text{FvK}}^0 + \bar{\boldsymbol{\beta}} \boldsymbol{\kappa} + \bar{\boldsymbol{\gamma}}(\lambda) \\ \mathbf{M} &= \bar{\boldsymbol{\alpha}} \mathbf{E}_{\text{FvK}}^0 + \bar{\boldsymbol{\beta}} \boldsymbol{\kappa} + \bar{\boldsymbol{\gamma}}(\lambda) \end{aligned} \quad (3)$$

here $\bar{\boldsymbol{\alpha}}$, $\bar{\boldsymbol{\beta}}$, $\bar{\boldsymbol{\gamma}}$, $\bar{\boldsymbol{\alpha}}$, $\bar{\boldsymbol{\beta}}$, $\bar{\boldsymbol{\gamma}}$ denote auxiliary functions that are defined in Section S3 (Supporting Information), see Equations (S5)–(S7) (Supporting Information). The system can be decoupled

by choosing that the reference plane coincides with the neutral plane, so that $\bar{\boldsymbol{\beta}} = \bar{\boldsymbol{\alpha}} = \mathbf{0}$. Yet, the residual stresses due to pre-stretch will still be relaxed through both, the in-plane and the out-of-plane deformations.

Furthermore, due to the stress free boundary conditions, and to reduce the number of unknowns, it is advantageous to formulate the problem in terms of vertical displacements and a stress function, rather than vertical and in-plane displacements. Therefore, we define an Airy stress function \mathcal{F} , so that it satisfies the in-plane equilibrium condition,^[36] By the restrictions of the in-plane compatibility conditions, an additional condition on \mathcal{F} must hold,

$$\Delta^2 \mathcal{F} + \frac{\bar{\alpha}(1 - \bar{\nu}_A^2)}{2} [w, w] = 0 \quad (4)$$

where $[\cdot, \cdot]$ is the Monge-Ampere operator,^[36] Furthermore, the out-of-plane displacement w has to satisfy the out-of-plane equilibrium conditions,

$$\bar{D} \Delta^2 w - \nabla \cdot (\bar{\nabla} \bar{\nabla} \mathcal{F} \nabla w) = 0 \quad (5)$$

where \bar{D} is the bending rigidity.

4.1. Uncut Symmetric Solution

Following experimental results shown in Figure 3, we first seek an axi-symmetric solution, which we refer to as a “cup”. The theory suggests that after the prestretched and nonprestretched layers are joined, the membrane stresses are equilibrated in both layers after the release, but due to the coupling between membrane stresses in the mid-surface of each layer, bending moments are induced. These lead to the shortening and compressive (circular) membrane forces in the circumference of the two-layered circular composite plate, most prominently toward the edge. By plane equilibrium, tensile membrane forces are induced around the center of the plate, see Figure S3 (Supporting Information). From experiments and simulations described earlier we learn that increasing the prestretch increases the compressive (circular) membrane forces that cause the axisymmetric cup structure to lose its stability and wrinkle (bend) into a k -fold axisymmetric structure to release the total strain energy.

4.2. k -Fold Axisymmetric Postbuckling

We next seek the k -fold axisymmetric solution with the following two model functions $w(r, \theta) = \bar{w}(r) + \tilde{w}(r, \theta)$ and $\mathcal{F}(r, \theta) = \bar{\mathcal{F}}(r) + \tilde{\mathcal{F}}(r, \theta)$. Here, $\bar{w}(r) = \int \varphi(r) dr$ and $\bar{\mathcal{F}}(r) = \int \phi(r) dr$ are the axisymmetric solutions from Section 4.1, while $\tilde{w}(r, \theta) = f(r) \cos k\theta$ and $\tilde{\mathcal{F}}(r, \theta) = g(r) \cos k\theta$ describe the k -fold axisymmetry. Note that model functions $w(r, \theta)$ and $\mathcal{F}(r, \theta)$ solve linearized version of Equations (S15)–(S16) (Supporting Information) exactly, which means that they also represent a viable solution in the immediate postbuckling. Obtained equations for $f(r)$ and $g(r)$ are solved numerically for different prestretches λ .

In Figure 4A, we present a maximum displacement normalized with the composite radius w_{max}/a in a series of energetically

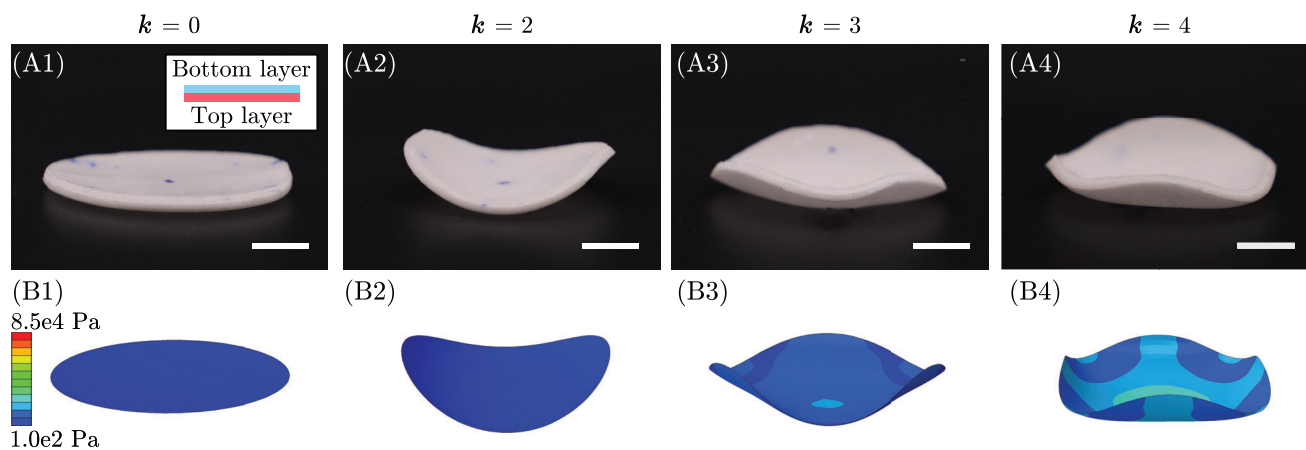


Figure 3. Free buckling shapes of soft composites. A) Experimental images and B) snapshots from finite element simulations at different values of prestretch: 1) $\lambda = 1.015$, 2) $\lambda = 1.064$, 3) $\lambda = 1.108$, and 4) $\lambda = 1.167$ to obtain different number of waves ($k = 0, 2, 3$, and 4, respectively) on the outer edge. Scalebar: 1 cm. For experimental parameters and finite element simulations are described in Supporting Information.

favorable wrinkling modes as a function of prestretch λ . Configurations with the lowest total strain energy E_{tot} as a function of λ are shown in Figure 4B. For smaller λ we observe first a twofold symmetric (Pringles chip-like) mode, followed by threefold, fourfold, etc. symmetric solutions, when the prestretch is increased. This solution indicates that the wrinkling mode (i.e., its wavenumber) increases with the applied prestretch, similar to what Stein-Montalvo et al.^[32] reported for buckling of confined shells. The reason for the favorization of higher wavenumber modes at higher prestretches is that they more effectively release the membrane strain energy by localizing bending at the edge of the plate, while they do not increase the bending strain energy around the center of the plate, cf. Figure S3 (Supporting Information). In other words, if a lower mode would be forced to remain under increased prestretch conditions it could only equilibrate an increased load by increasing its amplitude, which also affect the inner region of the plate in radial direction, where membrane forces are strictly tensile.

Another reason why the higher deformation modes k are promoted with larger prestretches λ is that the increasing curvature of the system (cup solution) provides geometric rigidity, which acts in this case analogously to an elastic substrate for edge concentrated wrinkles. However, our experiments and computations show that higher wavenumber k and edge localized bending deformation are no longer energetically favorable when the prestretch is very large.

4.3. Deep Postbuckling

Induced by a very large prestretch, a cylindrical bending solution (which we refer to as a “scroll”) becomes energetically favorable. This reduces Equation (5) to $\kappa_{11,11} = 0$, as only $\kappa_{11} \neq 0$ and $\kappa_{22} = \kappa_{12} = 0$, while Equation (4) is automatically satisfied. Assuming stress free edges, we obtain $\mathbf{N} = \mathbf{0}$ and $\kappa_{11} = \gamma_0/\bar{D}$, where the parameters γ_0 and \bar{D} are defined in Equation (S9) (Supporting Information). In this configuration, the membrane stresses are released entirely, at the price

of larger bending strain energy. However, the total strain energy is still smaller and simplified to $\mathcal{E} = \pi a^2 \gamma_0^2 / (2\bar{D})$.

5. Soft Kirigami Composites

Informed by the nonlinear nature of the problem and the existence of multiple branches in the previous section, we look for a way of reaching the hemispherical cap solution without the loss of stability and with sufficient axis-symmetry. As opposed to the 1D example,^[28,37] where applying any prestretch always yields a circular arch, compressive forces that occur on the circular plate due to the change of circumference during bending, avert the circular plate to bend into a hemisphere,^[32,38] and rather promote k -fold wrinkling instabilities or a scroll solution at really large prestretch. Intuitively, to achieve a targeted 3D topography, such as hemispherical cap, some material has to be removed to release the compressive forces – on exactly one layer for the self-assembly option. This partially removes the tendency of the outer edge of the composite to wrinkle through reduction of the compressive membrane stresses in the structure.

Therefore, to fabricate a spherical cap of a specific height, a certain amount of material corresponding to the circular angle $2\pi\alpha$ has to be removed. Since the problem is not governed only by the geometry, but also elasticity of the substrate, an exact amount of α cannot be determined directly from the desired geometry of the cap. To achieve a high axial symmetry, intuition also suggests to make a high number of cut-outs n_c from the kirigami layer, each cut-out being $2\pi\alpha/n_c$ in size. Note that these cut-outs impose an immediate n_c -fold symmetric shape in the (whole) composite structure without buckling transition. However, it turns out that too many cuts promote wrinkling instabilities in the composite, but too few impair its axisymmetry. Therefore, we search for the appropriate cutting parameters α and n_c to ensure that the n_c -fold symmetric structure is stable and axisymmetric (hemispheric).

To experimentally realize this observation, we chose a kirigami layer with $n_c = 10$ cuts. Figures 5B,C show the shapes of a soft kirigami composite at different values of prestretch from experiments and simulations. At small values of prestretch, $\lambda = \{1.05,$

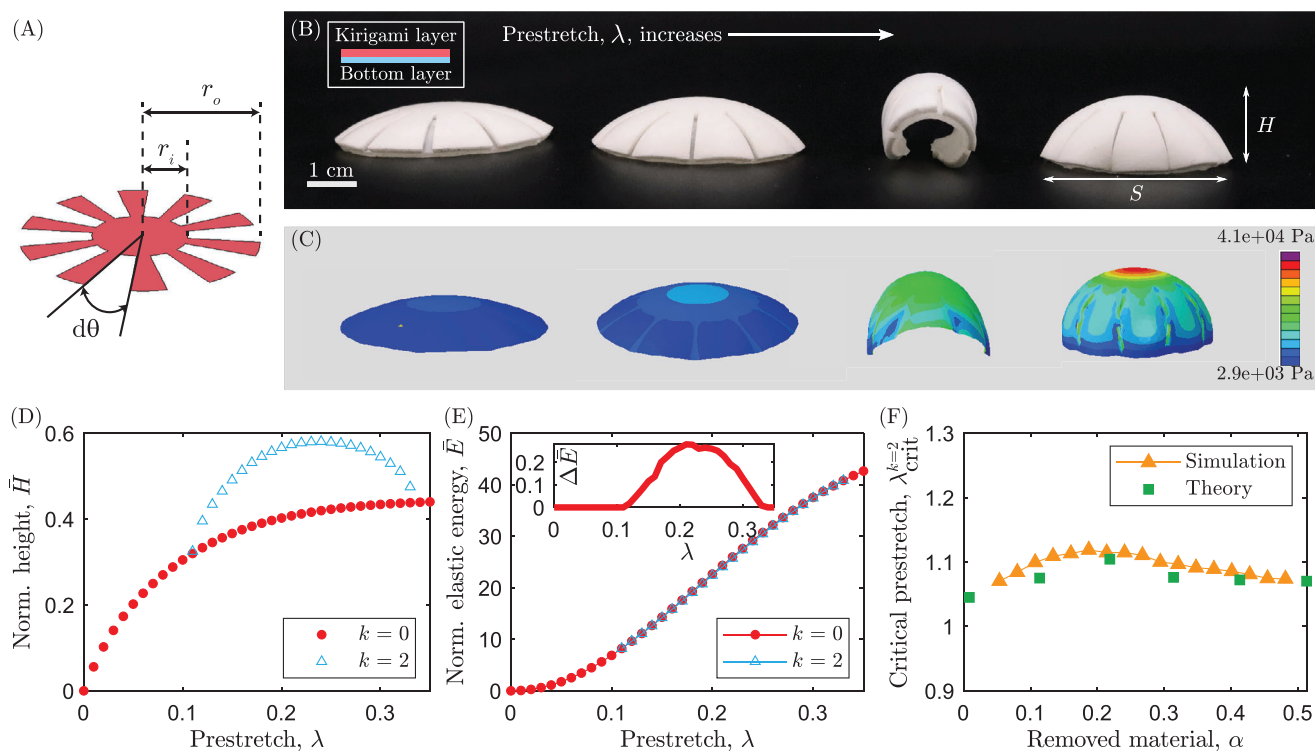


Figure 5. Soft kirigami composites. A) Geometric parameters of kirigami layer: cutout angle: $d\theta$, inner radius r_i , and outer radius, r_o . B) Experimental images and C) snapshots from finite element simulations at different values of prestretch: 1) $\lambda = 1.05$, 2) $\lambda = 1.15$, 3) $\lambda = 1.2$, and 4) $\lambda = 1.25$ to obtain the preprogrammed shapes. It turns out that a (quasi)axisymmetrical shape is not energetically favorable for $1.15 \lesssim \lambda \lesssim 1.25$ for this particular set of material and geometric parameters. D) Normalized height, $\bar{H} = H/R_o$, as a function of prestretch, λ , where R_o is the radius of the kirigami layer. E) Normalized strain energy, \bar{E} , as a function of λ at two different mode shapes: $k=0$ and $k=2$. The strain energy has been normalized by the characteristic bending energy, as described in the text. The inset shows the difference in normalized strain energy between the two ($\Delta\bar{E} = \bar{E}_{k=0} - \bar{E}_{k=2}$, where the subscript indicates the mode number) as a function of λ . F) Critical prestretch, $\lambda_{\text{crit}}^{k=2}$, as a function of the portion of the removed material, α ($\alpha = 1$ means the entire layer has been removed). For experimental parameters see Section 2.1.

1.15], the composite exhibits $n_c = 10$ -fold symmetry. However, as the prestretch increases to $\lambda = 1.2$, the structure undergoes buckling transition and assumes a twofold wrinkled form. Surprisingly, our results show in Figure 5B,C that if the prestretch is further increased to $\lambda = 1.25$, the previous symmetry (found at very small prestretch) is regained and a deeper hemispherical cap is formed.

We, first, numerically analyze the finding. Figure 5D,E show the height, H , of the kirigami composite and the elastic energy, E , as functions of prestretch, λ . The height has been normalized by the radius of the substrate ($R = 2$ cm) so that $\bar{H} = H/R$. The strain energy has been normalized by the characteristic elastic energy of the composite as discussed in Section 2.1. The difference in energy between two different modes ($k=0$ and $k=2$) is too small to be visually observable from the full-scale diagram, therefore, Figure 5E includes an inset showing the normalized difference in strain energy between the two modes: $\Delta\bar{E} = \bar{E}_{k=0} - \bar{E}_{k=2}$. Note that $\Delta\bar{E}$ is positive between $1.15 \lesssim \lambda \lesssim 1.30$; i.e., $k=2$ is energetically favorable compared with the “cup” solution corresponding to $k=0$ mode. Similar to our analysis of uncut composites presented above, we strive for an understanding of the interplay between deformation and cutting parameters of the kirigami layer (n_c, α).

We now modify our theory above to account for 1) the reduction of effective bending and membrane stiffness due to the cut-out material and 2) membrane forces relaxation due to additional bending of the cut-out sectors. For the calculation of the effective membrane and bending stiffness reduction of the soft kirigami composite, we assume that we have n_c disk sectors of the polar angle $2\pi\alpha/n_c$, where kirigami layer has been cut out (only substrate), and n_c disk sectors of the polar angle $2\pi(1-\alpha)/n_c$ with both layers. Effectively, we can model such structure as a layered composite of multiple sub-domains with both layers and sub-domains of only substrate layer. The domains can be viewed as parallelly connected in the radial direction and connected in series in the circular direction of the composite. From here, the effective membrane and bending stiffness of the soft kirigami substrate can be calculated as for the regular layered composite materials.^[39] The effective transversely anisotropic bending stiffness in the radial direction is therefore a weighted sum $D_{rr} = \alpha D^{\text{sub}} + (1-\alpha)D^{\text{both}}$ (analog to parallel springs), while the anisotropic bending stiffness in the circular direction is $D_{\theta\theta} = (\alpha/D^{\text{sub}} + (1-\alpha)/D^{\text{both}})^{-1}$ (analog to serial springs). Hereafter, the superscript ^{sub} indicates parameters of the substrate and ^{both} represents combined properties of the substrate/kirigami composite. Note that in both expressions the effective stiffness

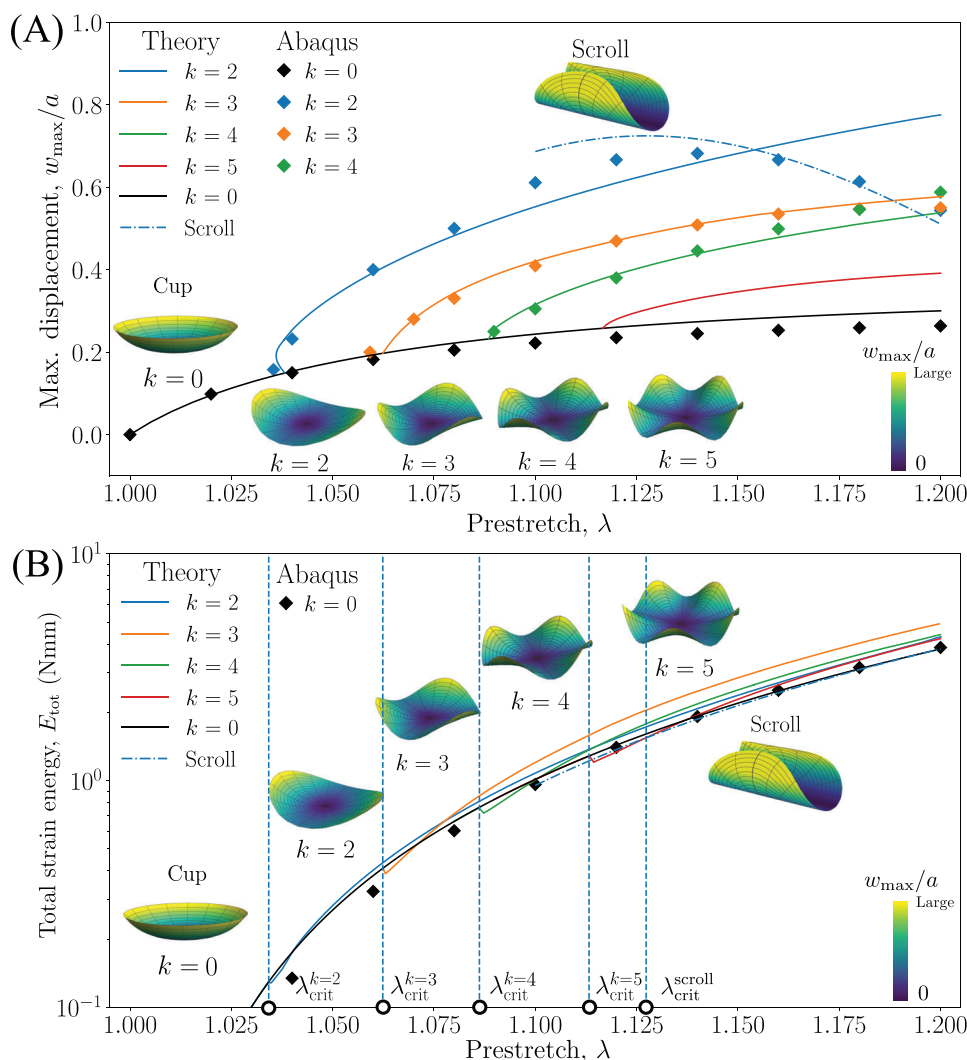


Figure 4. k -fold axisymmetric postbuckling solutions. Theoretical (lines) and numerical (diamonds) solution for bending and wrinkling of soft circular composites for different prestretches of the substrate λ . Panel A shows the maximum vertical displacements of different branches of solutions $k = \{0, 2, 3, 4, 5\}$ (solid lines and diamonds) and the scroll solution (dash-dotted lines and diamonds). Panel B shows the total strain energies for different branches of solutions. The “cup” axis-symmetric solution branch $k = 0$ exists for all prestretches λ , however different k -fold axisymmetric solutions might be energetically more favorable at some λ . The axisymmetric deformation mode $k = 0$ is preferable in the range $\lambda_0 = [1, 1.0381)$, the *two*fold axisymmetric mode in the range $\lambda_2 = [1.0381, 1.0608)$ etc. From $\lambda = 1.128$ on, the scroll deformation mode is energetically preferable.

decreases with increasing cut ratio α and does not depend on the number of the cutouts n_c . Analogous expressions can be written for the membrane stiffness. The effective Poisson’s ratio is $\nu_{\text{eff}} = (\alpha/\nu^{\text{sub}} + (1 - \alpha)/\nu^{\text{both}})^{-1}$.

The relaxation of the compressive membrane forces in the soft kirigami composite is a result of additional bending in the circumferential direction of the i -th disk sector (i represents a sector with only substrate or with both layers). We include this additional bending and with it the relaxation of membrane forces into account by assuming that the bending of the circular sectors is piecewise linear. The magnitude of such bending deformation can be calculated from a) the n -fold circular symmetry of the cut composite and b) the continuity of stresses and the continuity of deformations. The plate is still modeled as a composite plate, where the reduction of structural stiffness affects both the out of

plane equilibrium and the in-plane compatibility, while the relaxation of membrane forces mainly affects the in-plane compatibility conditions. The obtained leading equations are analogous to Equations (4) and (5), but differ due to the anisotropy and relaxation of the membrane forces due to bending of the kirigami composite sectors. Therefore, we can use similar approach to solution as in Section S3.1 (Supporting Information).

5.1. Effect of Kirigami on Compressive Membrane Forces

We first search for n_c -fold axisymmetric “cup” solution, similar to that in Section 4.1. By averaging the nonlinear terms and using the same model function as for the “cup” solution, $\varphi(r) = C_1(r/a)^n$, we can calculate approximately the membrane

stresses from the in-plane compatibility Equation (4) for the anisotropic case.

From this approach, we find that for a fixed prestretch λ , increasing α decreases bending stiffness $D_{\theta\theta}$ and D_{rr} , and increases angle φ , which deepens the “cup”. The deepening of the “cup” reduces the circumference of the “cup” and therefore increases the membrane forces. On the other hand, bending of the disk sectors in the circular direction increases the circumference of the “cup” and releases some of the membrane forces. Furthermore, if the number of cut circular sectors is small, e.g., $n_c \rightarrow 2$, then increasing the cutout ratio α causes large bending of the sectors and the membrane forces become smaller, see Figure S4 (Supporting Information). Such structure is less prone to losing its stability, but lacks axisymmetry. As already mentioned, the axisymmetry is increased with increasing n_c . In this case, the circumferential bending of the sectors does not decrease the membrane forces significantly.

5.2. Buckling Resilience of Soft Kirigami Composite

Next, we analyze the kirigami composite structure “buckling resilience”, by posing an alternative problem of loading a stress-free composite kirigami “cup” shell with a constant homogeneous compressive membrane force $N_0 = N_0 I$. We define buckling resilience as a magnitude of the membrane force N_0^{crit} needed for this structure to lose its stability and wrinkle. It is related to bending rigidity, induced geometric rigidity due to the curvature of the “cup”, and the fact that the structure can only wrinkle in a discrete number of wrinkling modes that have to comply with the boundary conditions and depend on the size of α and n_c . The system is solved numerically via finite element method for different α and n_c , where we fix λ .

From this alternative analysis (see Figure S5, Supporting Information) we can see, that for small number of cuts, e.g., $n_c \rightarrow 4$, increasing α decreases the bending rigidity, but increases the geometric rigidity due to the deepening of the “cup”. The overall buckling resilience therefore increases until $\alpha \lesssim 0.2$ and after that it slowly degrades. However, for a larger number of cuts, e.g., $n_c \rightarrow 20$, buckling resilience increases slightly only until $\alpha \lesssim 0.1$, and then decreases substantially. In the limit, as $n_c \rightarrow \infty$, we essentially obtain a homogenized anisotropic structure with reduced bending rigidity and reduced buckling resilience.

5.3. Designing a Stable Hemispherical Kirigami Cup

From the analysis of membrane forces and buckling resilience analyzed in previous subsections, we now understand that a low number of cutouts, e.g., $n_c \rightarrow 4$, causes a large relaxation of compressive membrane forces due to circular bending of sectors and deepening of the “cup” that induce geometric rigidity, which suppresses loss of stability (i.e., transition to the $k = 2$ mode). The obtained “cup” is relatively stable, but not highly axisymmetric. Such structures are explicitly shown in Figure S6 (Supporting Information), as reduced membrane forces and increased buckling resilience do not allow the “cup” structure to lose its stability and transition to the $k = 2$ mode. On the other hand, a large number of cutouts, as $n_c \rightarrow \infty$, induce a highly axisymmetric “cup”, however the membrane forces increase, while the buckling resilience

decreases significantly, which pushes the structure to $k = 2$ configuration already at lower λ .

Turning back to the real loading conditions of our soft kirigami composite, we further study how the cutout ratio α affects the threshold λ_{crit} for the loss of stability on $n_c = 10$ structure (n_c was chosen as a compromise between axisymmetry and stability). We again resort to numerical eigenvalue analysis, where this time N_0 and κ_0 are calculated depending on the prestretch λ and cutting parameters α and n_c . The results, compared graphically with the results from numerical simulations in Abaqus shown in Figure 5F indicate that there exists an optimal α (at ≈ 0.2 for given geometric, material and cutting parameters), where the critical prestretch $\lambda_{\text{crit}}^{k=2}$ is the largest. However, it is not large enough to attain a pure hemispherical shape without buckling to $k = 2$ configuration first. Counterintuitively, one may rather cut the structure many times to reach a high axisymmetry and with a large cutout ratio α to lower all the critical prestretches $\lambda_{\text{crit}}^{k \leq n_c}$ – so much that the structure will buckle into $k = n_c$ -fold axisymmetric deformation mode to form a quasi-hemisphere. Technically such structure is still wrinkled, but because the number of cuts is large enough the wrinkled shape is close to being axisymmetric.

An example of such structure is given in Figure 5B,C, where the prestretch is applied to a structure with $n_c = 10$ cutouts and $\alpha = 0.13$. In the first and second case, the applied prestretches are lower than the critical $\lambda_{\text{crit}}^{k=2}$, while in the third case it is larger, just enough to make the structure to assume the “scroll” form. Upon increasing the prestretch further, the structure assumes the hemispherical shape in the fourth case, i.e., when the prestretch just surpasses $\lambda_{\text{crit}}^{k=10}$ and the structure forms a stable tenfold hemispherical axisymmetrical shape. From these results, we speculate that the mechanical response of the soft kirigami structure is qualitatively the same as for the uncut soft circular composite plate, except $\lambda_{\text{crit}}^{k=n_c}$ and strain energy are decreased, for the kirigami composite structure.

6. Conclusion

We have introduced the combination of kirigami and prestretch as a pathway toward self-assembly of targeted 3D shapes. Our theoretical analysis and numerical simulations reveal a complex energy landscape consisting of multiple stable solutions that depends on several geometric and material parameters. To precisely control such a large number of parameters, we developed an experimental device that can apply fully homogeneous prestretch. Furthermore, the entire fabrication process happens in a 2D plane, which significantly reduces manufacturing costs and indicates potential usage in scaled-up industrial applications, for example self-erecting tents, soft carriers for flexible solar panels and self-assembling antennas.

Despite our ability to precisely control the associated cutting parameters and prestretch, achieving targeted 3D shapes requires solving an inverse problem to compute the desired parameters. In this paper, we adopted hemispherical cap as our target and presented experimental, numerical, and theoretical analyses to fabricate soft composites of such shapes. In this process, we found that cutting parts of a layer can be used to release compressive stresses and prevent unwanted warping. We found guidelines on how to choose the appropriate cutting

parameters (e.g., cutout ratio and the number of cuts) to design a (quasi)-axisymmetric hemisphere. Even though we focused on axisymmetric targets in this study to benefit from theoretical simplifications, the gained insights can be coupled with numerical methods in the future to obtain arbitrary 3D topographies not restricted to hemispheres. This can be achieved either by applying a non-symmetric kirigami, see Figure S1 and Section S1 (Supporting Information), or by applying the prestretch locally across the surface, see,^[40] and carefully prescribing the cuts in the kirigami layer.

Supporting Information

Supporting Information is available from the Wiley Online Library or from the author.

Acknowledgements

J.Z. and Y.W. contributed equally to this work. The authors acknowledged financial support from the National Science Foundation (Grants: CAREER-2047663, CMMI-2053971, IIS-1925360, and CMMI-2101751) and Slovenian Research Agency (Grants: J2-9223, J2-2499, and J2-4449). The authors also thank Kellen Cheng for help with preliminary experiments.

Conflict of Interest

The authors declare no conflict of interest.

Data Availability Statement

Data sharing is not applicable to this article as no new data were created or analyzed in this study.

Keywords

kirigami, morphing, prestretch, shell buckling

Received: June 5, 2023

Revised: October 19, 2023

Published online:

- [1] S. Xu, Z. Yan, K.-I. Jang, W. Huang, H. Fu, J. Kim, Z. Wei, M. Flavin, J. McCracken, R. Wang, A. Badea, Y. Liu, D. Xiao, G. Zhou, J. Lee, H. U. Chung, H. Cheng, W. Ren, A. Banks, X. Li, U. Paik, R. G. Nuzzo, Y. Huang, Y. Zhang, J. A. Rogers, *Science* **2015**, *347*, 154.
- [2] J. Panetta, M. Konaković-Luković, F. Isvoranu, E. Bouleau, M. Pauly, *ACM Trans. Graph. (TOG)* **2019**, *38*, 1.
- [3] K. Sim, S. Chen, Z. Li, Z. Rao, J. Liu, Y. Lu, S. Jang, F. Ershad, J. Chen, J. Xiao, C. Yu, *Nat. Electron.* **2019**, *2*, 471.
- [4] J. Pikul, S. Li, H. Bai, R. Hanlon, I. Cohen, R. F. Shepherd, *Science* **2017**, *358*, 210.
- [5] Y. Wang, S. Hu, T. Xiong, Y. Huang, L. Qiu, *Struct. Health Monit.* **2022**, *21*, 2453.
- [6] M. Ding, L. Jing, H. Yang, C. Machnicki, X. Fu, K. Li, I. Wong, P.-Y. Chen, *Mater. Today Adv.* **2020**, *8*, 100088.
- [7] J. Betts, *Endeavour* **1993**, *17*, 160.
- [8] S. Conti, A. DeSimone, G. Dolzmann, *J. Mech. Phys. Solids* **2002**, *50*, 1431.
- [9] M. O. Saed, C. P. Ambulo, H. Kim, R. De, V. Raval, K. Searles, D. A. Siddiqui, J. M. O. Cue, M. C. Stefan, M. R. Shankar, T. H. Ware, *Adv. Funct. Mater.* **2019**, *29*, 1806412.
- [10] A. M. Abdullah, X. Li, P. V. Braun, J. A. Rogers, K. J. Hsia, *Adv. Funct. Mater.* **2020**, *30*, 1909888.
- [11] L. Ionov, *Adv. Funct. Mater.* **2013**, *23*, 4555.
- [12] J. J. Wie, M. R. Shankar, T. J. White, *Nat. Commun.* **2016**, *7*, 1.
- [13] X. Ni, H. Luan, J.-T. Kim, S. I. Rogge, Y. Bai, J. W. Kwak, S. Liu, D. S. Yang, S. Li, S. Li, Z. Li, Y. Zhang, C. Wu, X. Ni, Y. Huang, H. Wang, J. A. Rogers, *Nat. Commun.* **2022**, *13*, 1.
- [14] T. S. Shim, S.-M. Yang, S.-H. Kim, *Nat. Commun.* **2015**, *6*, 1.
- [15] E. Siéfert, E. Reyssat, J. Bico, B. Roman, *Nat. Mater.* **2019**, *18*, 24.
- [16] D. Ambrosi, M. Ben Amar, C. J. Cyron, A. DeSimone, A. Goriely, J. D. Humphrey, E. Kuhl, *J. R. Soc., Interface* **2019**, *16*, 20190233.
- [17] L. Zhang, S. Chizhik, Y. Wen, P. Naumov, *Adv. Funct. Mater.* **2016**, *26*, 1040.
- [18] Y. Tang, Y. Li, Y. Hong, S. Yang, J. Yin, *Proc Natl. Acad. Sci.* **2019**, *116*, 26407.
- [19] J. Cui, F. R. Poblete, Y. Zhu, *Adv. Funct. Mater.* **2018**, *28*, 1802768.
- [20] N. An, A. G. Domel, J. Zhou, A. Rafsanjani, K. Bertoldi, *Adv. Funct. Mater.* **2020**, *30*, 1906711.
- [21] D. Dureisseix, *Int. J. Space Struct.* **2012**, *27*, 1.
- [22] B. Davidovitch, R. D. Schroll, D. Vella, M. Adda-Bedia, E. A. Cerda, *Proc. Natl. Acad. Sci.* **2011**, *108*, 18227.
- [23] G. M. Grason, B. Davidovitch, *Proc. Natl. Acad. Sci.* **2013**, *110*, 12893.
- [24] B. Davidovitch, Y. Sun, G. M. Grason, *Proc. Natl. Acad. Sci.* **2019**, *116*, 1483.
- [25] M. Liu, L. Domino, D. Vella, *Soft Matter* **2020**, *16*, 7739.
- [26] Z. Fan, Y. Yang, F. Zhang, Z. Xu, H. Zhao, T. Wang, H. Song, Y. Huang, J. A. Rogers, Y. Zhang, *Adv. Mater.* **2020**, *32*, 1908424.
- [27] M. Pezulla, S. A. Shillig, P. Nardinocchi, D. P. Holmes, *Soft Matter* **2015**, *11*, 5812.
- [28] M. Pezulla, G. P. Smith, P. Nardinocchi, D. P. Holmes, *Soft Matter* **2016**, *12*, 4435.
- [29] M. Pezulla, N. Stoop, X. Jiang, D. P. Holmes, *Proc. R. Soc. A* **2017**, *473*, 20170087.
- [30] M. Pezulla, N. Stoop, M. P. Steranka, A. J. Bade, D. P. Holmes, *Phys. Rev. Lett.* **2018**, *120*, 048002.
- [31] A. DeSimone, *Meccanica* **2018**, *53*, 511.
- [32] L. Stein-Montalvo, P. Costa, M. Pezulla, D. P. Holmes, *Soft Matter* **2019**, *15*, 1215.
- [33] E. Cerda, K. Ravi-Chandar, L. Mahadevan, *Nature* **2002**, *419*, 579.
- [34] A. F. Bower, *Applied mechanics of solids*, CRC press, Boca Raton **2009**.
- [35] L. D. Landau, L. P. Pitaevskii, E. M. Lifshitz, A. M. Kosevich, *Theory of Elasticity*, 3 edition, Butterworth-Heinemann, Oxford **1986**.
- [36] C. D. Coman, *Appl. Math. Lett.* **2012**, *25*, 2407.
- [37] P. Nardinocchi, E. Puntel, *Int. J. Solids Struct.* **2016**, *90*, 228.
- [38] H. Bense, M. Trejo, E. Reyssat, J. Bico, B. Roman, *Soft Matter* **2017**, *13*, 2876.
- [39] W. Callister, *Materials Science and Engineering: An Introduction*, Wiley, Hoboken, New Jersey, USA **1997**.
- [40] E. Annevelink, H. T. Johnson, E. Ertekin, *Curr. Opin. Solid State Mater. Sci.* **2021**, *25*, 100893.